6th World Congress on Structural and Multidisciplinary Optimization
Rio de Janeiro, 30 May - 03 June 2005, Brazil

An Image Segmentation Method Based on a Discrete Version of the Topological Derivative

I. Larrabide[1], R.A. Feijóo[1], A.A. Novotny[1],E. Taroco[1] & M. Masmoudi[2]

[1] Laboratório Nacional de Computação Científica LNCC/MCT,
Av. Getúlio Vargas 333, 25651-075 Petrópolis - RJ, Brasil
[2] Mathématiques pour l'Industrie et la Physique UMR 5640,
Université Paul Sabatier, 118, route de Narbonne,
31062 Toulouse cedex 4, France

1. Abstract
Computed tomography (CT) and magnetic resonance imaging (MRI) have introduced 3D data sets into clinical radiology. 3D data sets provide information for analysis not available in 2D imaging and challenge the traditional 2D viewing and interpretation used in most clinical environments. Despite the 3D format of CT and MRI, they are largely interpreted and analyzed as individual 2D image slices. One of the most important stages in medical image analysis is segmentation of objects or definition of their contours. Although improving imaging techniques (e.g., contrast agents, biological markers) should facilitate the segmentation process, medical images are relatively difficult to segment for several undesired properties like low signal-to-noise and contrast-to-noise ratios and multiple and discontinuous edges. Our aim in this paper is to present an image segmentation method based on a discrete version of the well established concept of topological derivative. More specifically, we compute the topological derivative for an appropriate functional associated to the image indicating the *cost* endowed to an specific image segmentation. Further, we propose an image segmentation algorithm based on this approach. Finally, some results are presented in order to show the computational performance of this methodology.
2. Keywords: Topological derivative, medical images, segmentation.

3. Introduction

Medical imaging techniques such as Ultrasound, Magnetic Resonance Imaging (MRI) or Computed Tomography (CT) provide detailed 3D images of human internal organs. 3D data sets provide information for analysis not available in 2D imaging and at the same time challenge the traditional 2D viewing and interpretation used in most clinical environments. Despite their 3D format both CT and MRI, are largely interpreted and analyzed as individual 2D image slices. Quantitative information such as organ size and shape can be extracted from these images in order to support activities such as disease diagnosis and monitoring and surgical planning. However, in order to accomplish this, the first step we must do is to identify the different tissues and anatomical structures being involved. This process, called segmentation, must be accurate and repeatable in order to be clinically useful.

Segmentation subdivides an image into its constituent regions or objects. The level to which the subdivision is carried depends on the problem being solved. For example, in the segmentation of medical images, the objective is to identify different regions, organs and anatomical structures from data acquired via CT, MRI, Ultrasound or other medical imaging technique.

Classical image segmentation techniques are based on two basic pixel* characteristics: discontinuities and similarities. Many of this classical techniques (e.g., multiple thresholding, region growing, morphologic filtering and others [5, 8]) have been applied to try to solve this problem with variable outcomes [7, 14]. Such techniques tend to be unreliable when segmenting a structure that is surrounded by others with similar image intensity (eg, low-contrast structures).

More sophisticated techniques, like level sets, use powerful numerical computations for tracking the evolution of moving surface fronts. These techniques are based on computing linear/nonlinear hyperbolic equation system solutions for the appropriate equations of motion. An initial approximation of the solution (seed) evolves until it gets the limits of the region of interest. In this case user interaction is needed to introduce one or more seeds (or starting points) for the algorithm to evolve [11, 12]. Although this approach brings good results, it's computational cost may become too high. A wide variety of works present the Active Contour (also called T-Snakes) technique as the most robust for medical image

*By pixel we mean picture element.

segmentation [1, 9, 15, 16]. With this technique good results are obtained, in particular for brain MRI segmentations, but input data must be pre-processed to extract spurious structures before the segmentation algorithm is started.

By means of Markov Random field in [6] and [17] are described fully automatic 3D-segmentation techniques especially designed for brain MRI images. This techniques captures three main spatial features of MRI images: non-parametric distribution of tissue intensities, neighborhood correlations and signal inhomogeneities. Once these fields are calculated (using suitable probabilistic models), an optimization algorithm (Iterated Conditional Modes, Simulated Annealing, Expectation-Maximization, etc.) is used to recalculate them until the algorithm converges. Again, the limitation of this technique is it's excessive computational cost.

Our aim in this paper is to present an automated image segmentation method based on a discrete version of the well established concept of topological derivative (see [2, 4, 10, 13] and references therein). More specifically, we compute the topological derivative for an appropriate functional associated to the image indicating the *cost* endowed to an specific image segmentation. Further, we propose an image segmentation algorithm based on this result. Finally, several image segmentations are presented in order to show the computational performance of this methodology.

4. Formal Definition for the Topological Derivative

The topological derivative allows us to quantify the sensitivity of the problem when the domain under consideration is perturbed by the introduction of a hole. More specifically, let Ω be an open set in $\mathbb{R}^N$ ($N = 2, 3$) and B_ϵ be a ball of radius ϵ centered at point $\tilde{x} \in \Omega$ (Figure 1). Taking into account a cost function Ψ, the associated topological derivative D_T can be defined as:

$$D_T(\tilde{x}) = \lim_{\varepsilon \to 0} \frac{\Psi\left(\Omega \backslash B_\varepsilon\right) - \Psi\left(\Omega\right)}{f\left(\varepsilon\right)} \,, \tag{1}$$

$$\Psi\left(\Omega \backslash B_\varepsilon\right) = \Psi\left(\Omega\right) + f\left(\varepsilon\right) D_T(\tilde{x}) + \ldots \tag{2}$$

where $f\left(\varepsilon\right)$ is a negative that decreases monotonically so that $f\left(\varepsilon\right) \to 0$ with $\varepsilon \to 0^+$. The topological

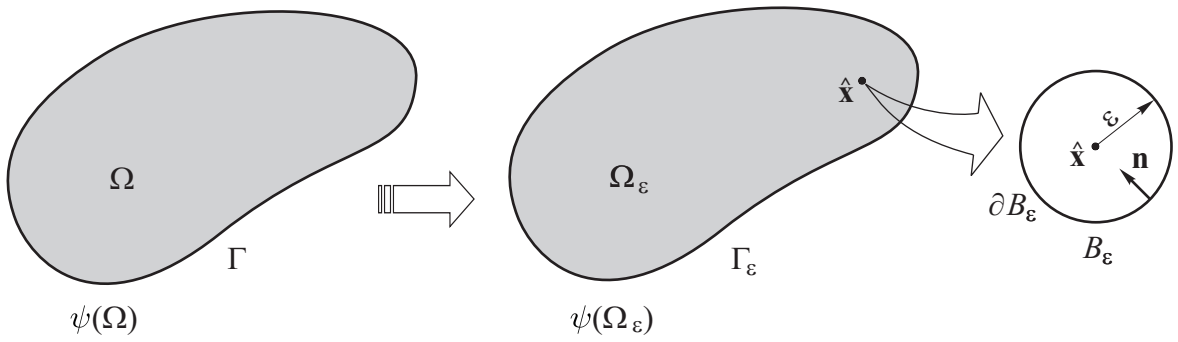

Figure 1: topological derivative concept

derivative D_T given by eq. (1) has been recognized as a powerful tool to solve topology optimization problems. Nevertheless, this concept is wider. In fact, extension of the topological derivative in order to consider arbitrary shaped holes and its applications to Navier, Laplace, Poisson, Helmoltz, Stokes, Navier-Stokes equations are developed by Masmoudi and by Sokolowsky and their co-workers. See also [3] for applications of the topological derivative to the above equations, inverse problems and material properties characterization. As already mentioned in this paper, we will introduce a discrete version for the topological derivative, which will be applied in the context of image segmentation.

5. Image Segmentation Problem

As in this work we deal with 3D images, therefore, the image will be characterized by a three-dimensional

matrix of voxels, instead of pixels. The difference between them is that a pixel only has height and width and a voxel has height, width and depth (3D element). For each image element (voxel) we associate an intensity according to the image type[†] and the technique used to acquire it. In addition, the image intensity is normalized assuming values from 0 to 1.

More specifically, let us consider a three-dimensional image characterized by an $M \times N \times Q$ matrix of voxels ω^{ijk}. For each voxel ω^{ijk} we respectively associate the intensities of the original image $u^{ijk} \in \mathcal{U}$, and segmented image $\bar{v}^{ijk} \in \mathcal{V}$, where the sets $\mathcal{U}$ and $\mathcal{V}$ are defined as:

$$\mathcal{U} := \{u^{ijk} \in \mathcal{I} : i = 1...N,\ j = 1...M,\ k = 1...Q\} , \tag{3}$$

$$\mathcal{V} := \{v^{ijk} \in \mathcal{C} : i = 1...N,\ j = 1...M,\ k = 1...Q\} . \tag{4}$$

Furthermore, the set $\mathcal{I}$ represents the normalized intensity values of the original image and the set $\mathcal{C}$ represents the intensities classes holding the solution of the segmentation. That is, the sets $\mathcal{I}$ and $\mathcal{C}$ are respectively defined as:

$$\mathcal{I}:=\{\rho \in \mathbb{R} : 0 \leq \rho \leq 1\} \quad \text{and} \quad \mathcal{C}:=\{c_s \in \mathcal{I} : s = 1...Nc\} , \tag{5}$$

where Nc is the number of classes and c_s represents a given class.

To identify a class different alternatives can be used. The values defined for the classes will depend on the cost function and the specific application of the segmentation. Therefore, we will obtain different results according to the criterion adopted to define the set of classes $\mathcal{C}$ (for instance, mean intensity or median intensity inside a region). In this work we used the mean intensity value inside a region to define the class that represents that region. Other *a priori* image information can be used to determine this values. In the case of CT the brighter intensities represent bone and darker areas represent soft tissues as inner organs or muscles. This information can be used to determine classes's characteristic values and appropriate cost function for the problem under consideration.

Finally, the image segmentation problem studied here can be stated as following: given the original image represented by the matrix $u^{ijk} \in \mathcal{U}$, the set of classes $\mathcal{C}$ and a specific cost function, find the segmented image represented by the matrix $\bar{v}^{ijk} \in \mathcal{V}$ such that minimizes the cost function.

5.1. Choosing the Cost Function

The election of the cost function depends on each particular problem. Let's focus our attention to medical image segmentation problem, whose main goal is to distinguish different tissues. In order to do this we could, for instance, characterize them by regions of homogeneous intensities. To achieve this goal we propose to minimize the following cost function:

$$\Psi = \theta\Phi + (1-\theta)\Gamma , \quad \text{with} \quad \theta \in (0,1] \subset \mathbb{R} , \tag{6}$$

where the first and second terms of the cost function Ψ, denoted by Φ and Γ, are associated with *distance* between the input image voxel's intensities u^{ijk} and the intermediate segmentation image voxel's intensities v^{ijk} and with the *contour measure*, respectively. In particular, these functions can be written as:

$$\Phi = \sum_{ijk} \int_{\omega^{ijk}} (u^{ijk} - v^{ijk})^2 \quad \text{and} \quad \Gamma = \frac{1}{4n} \sum_{ijk} \int_{\partial\omega^{ijk}} \chi(v^{ijk}) , \tag{7}$$

where n is the number of dimensions where the segmentation is being done and $\chi(v^{ijk})$ is a characteristic function that assumes the values 1 (one) over the boundary of voxels separating different classes and 0 (zero) otherwise. The θ parameter allows us to control the contribution of each term Φ and Γ in the cost function.

5.2. The Topological Derivative Computation

Now, we will compute the sensitivity of the cost function when we change the intensity of an arbitrary voxel $\omega^{\alpha\beta\gamma}$ from class $v^{\alpha\beta\gamma}$ to class c_s. Therefore, the perturbed cost function Ψ_s is given by:

$$\Psi_s = \theta\Phi_s + (1-\theta)\Gamma_s , \tag{8}$$

[†]RGB, Grayscale, 8bpp Grayscale, etc.

where Φ_s and Γ_s can be written as:

$$\Phi_s = \Phi - \int_{\omega^{\alpha\beta\gamma}} (u^{\alpha\beta\gamma} - v^{\alpha\beta\gamma})^2 + \int_{\omega^{\alpha\beta\gamma}} (u^{\alpha\beta\gamma} - c_s)^2 \ , \tag{9}$$

$$\Gamma_s = \Gamma - \frac{1}{4n} \int_{\partial\omega^{\alpha\beta\gamma}} \chi(v^{\alpha\beta\gamma}) + \frac{1}{4n} \int_{\partial\omega^{\alpha\beta\gamma}} \chi(c_s) \ , \tag{10}$$

Then the sensitivity, characterized by the topological derivative, in this discrete case is given by the difference $\Psi_s - \Psi$, that is:

$$D_T^s(\omega^{\alpha\beta\gamma}) = \theta \int_{\omega^{\alpha\beta\gamma}} \left[(u^{\alpha\beta\gamma} - c_s)^2 - (u^{\alpha\beta\gamma} - v^{\alpha\beta\gamma})^2\right] + (1-\theta)\frac{1}{4n} \int_{\omega^{\alpha\beta\gamma}} \left[\chi(c_s) - \chi(v^{\alpha\beta\gamma})\right]. \tag{11}$$

$$D_T^s(\omega^{\alpha\beta\gamma}) = \Psi(\omega^{\alpha\beta\gamma} \backslash c_s) - \Psi(\omega^{\alpha\beta\gamma}). \tag{12}$$

5.3. An Image Segmentation Algorithm

In this section we present the topological derivative segmentation algorithm for a 3D image (Algorithm 1). The algorithm inputs are the 3D image $u^{ijk} \in \mathcal{U}$ being segmented and a set of classes in witch the image will be segmented. The algorithm output is $\bar{v}^{ijk} \in \mathcal{V}$, corresponding to the class that voxel ω^{ijk} was classified. In fact, the topological derivative can be used as a descent criterion in an optimization process. Then, the sufficient local minimum condition for such voxel perturbation is given by:

$$D_T^s(\omega^{\alpha\beta\gamma}) \geq 0 \quad \forall\ \alpha = 1, \ldots, N \ ,\ \beta = 1, \ldots, M \ ,\ \gamma = 1, \ldots, Q \ and \ s = 1, \ldots, Nc \tag{13}$$

Moreover, our algorithm consists in evaluating the topological derivative for each voxel and each class. Then, the new (segmented) image is obtained by successively selecting for each voxel the class which produces the most negative value of the topological derivative at that voxel.

Algorithm 1 Image segmentation based on a discrete version of the Topological Derivative

Require: A 3D image $u^{ijk} \in \mathcal{U}$, the set of classes $\mathcal{C}$, and $\theta^* \in (0, 1]$
Ensure: The segmented image $\bar{v}^{ijk} \in \mathcal{V}$
  normalize the image and classes values
  take $\theta = 1$
  for every voxel $\omega^{\alpha\beta\gamma}$ **do**
    for every class $c_s \in \mathcal{C}$ **do**
      compute $D_T^s(\omega^{\alpha\beta\gamma})$ following (eq. 12)
    end for
    if $\min\{D_T^s(\omega^{\alpha\beta\gamma}),\ s = 1, \ldots, N_c\} < 0$ **then**
      $v^{\alpha\beta\gamma} = c_s$
    end if
  end for
  take $\theta = \theta^*$
  while $\exists$ s and $\alpha\beta\gamma$ such as $D_T^s(\omega^{\alpha\beta\gamma}) < 0$ **do**
    for every voxel $\omega^{\alpha\beta\gamma}$ **do**
      for every class $c_s \in \mathcal{C}$ **do**
        compute $D_T^s(\omega^{\alpha\beta\gamma})$ following (eq. 12)
      end for
      if $\min\{D_T^s(\omega^{\alpha\beta\gamma}),\ s = 1, \ldots, N_c\} < 0$ **then**
        $v^{\alpha\beta\gamma} = c_s$
      end if
    end for
  end while

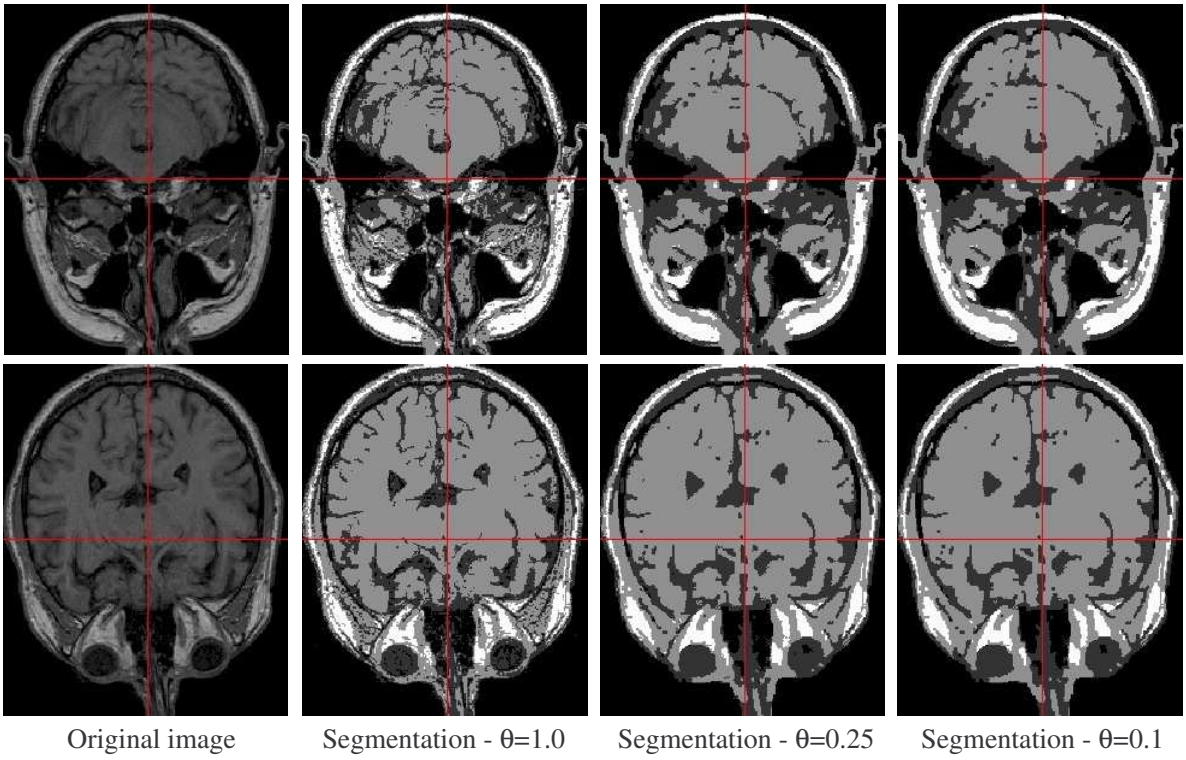

Figure 2: Segmentation for a head MRI.

6. Numerical Results

In the following subsections are presented some examples and results for different algorithm parameters.

6.1. 2D Images

6.1.1. Example 1

In the experiment was used a magnetic resonance corresponding to the brain. In this image we can observe different regions corresponding to the internal organs in the head. This characteristic simplifies the segmentation procedure and enhances the segmentation result. The original image presents 256 intensities (from 0 to 255). The classes's values used where 0, 30, 85 and 150.

In the first column of Figure 2 are presented two different planes of the original image. In the subsequent columns, are shown the same two planes in the resulting segmented image for $\theta = 1$, $\theta = 0.25$ and $\theta = 0.10$ respectively.

We can appreciate that in the case of $\theta = 1$ the segmentation presents non homogeneous regions. In other words, in regions where a class predominates there are (miss-classified) elements corresponding to another class. This first result was improved using $\theta = 0.25$, in this case the resulting segmentation has a better quality. In the last test was used $\theta = 0.10$, the segmentation in good, but some details where lost. In this case, $\theta = 0.10$ is too restrictive for this image having so much complex structures as the brain.

6.1.2. Example 2

In the second example was used a magnetic resonance corresponding to the head of a person with a brain tumor. This image presents complex and irregular structures corresponding to the brain and a tumor

of considerable proportions. The classes values used where 10, 60, 105, 140 and 200. The segmentation of this particular image becomes more difficult because of the envolved structures are complex and they present almost the same intensity.

In this case the image was segmented using different values for the algorithm's parameter θ. In the first column of Figure 3 are presented two different planes of the original image. In the sequel, are shown the corresponding planes of the resulting segmented image for $\theta = 1$, $\theta = 0.25$ and $\theta = 0.10$ respectively.

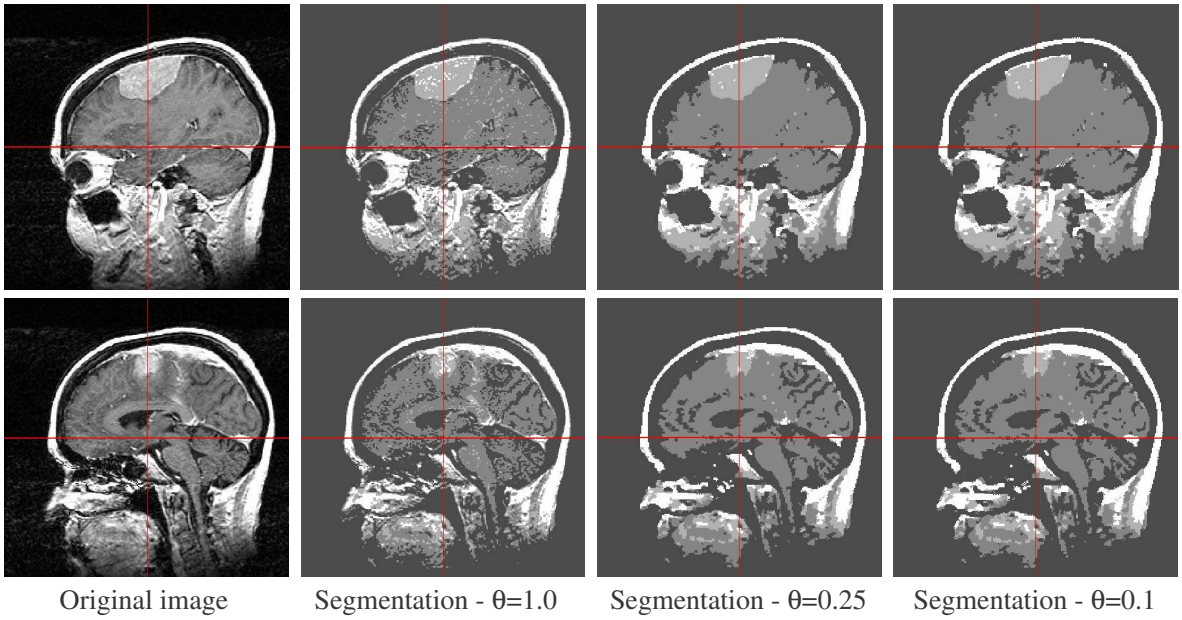

Figure 3: Segmentation for a head MRI.

We can appreciate that in the case of $\theta = 1$ the segmentation did not get all the details for the brain and some points were miss-classified. With parameter $\theta = 0.25$, the segmentation was enhanced considerably but there are still some points being miss-classified. Finally with $\theta = 0.10$ we get an acceptable result.

6.1.3. Example 3

In the last case was used a CT corresponding to an angiography from the region of the aorta. In this image we can observe two major regions corresponding to the head of the patient and to the contrasted[‡] arteries in the head. In this case we also have a good signal-to-noise and contrast-to-noise ratio that improves the segmentation result. The original image presents 1932 intensities (from 0 to 1931). The classes values used where 10, 70, 160 and 800.

In Figure 4 are presented two different planes corresponding to the original image and the same two planes for the segmentation results for $\theta = 1$, $\theta = 0.25$ and $\theta = 0.10$ respectively.

6.2. 3D Images

Once the regions and organs are segmented, it might be of interest (depending on the application) to three-dimensionally reconstruct the segmented structure for posterior visualization. The most popular algorithm for this means is Marching Cubes (MC). MC is an algorithm for iso-surface extraction from volumetric data like 3D images. The fundamental idea is to subdivide the data volume in cubes (voxels) that holds in its 8 vertices the information of intensity corresponding to those points in the 3D image.

[‡]In angiographies, a radioactive agent is injected in the blood flow to give better contrast to the blood vessels.

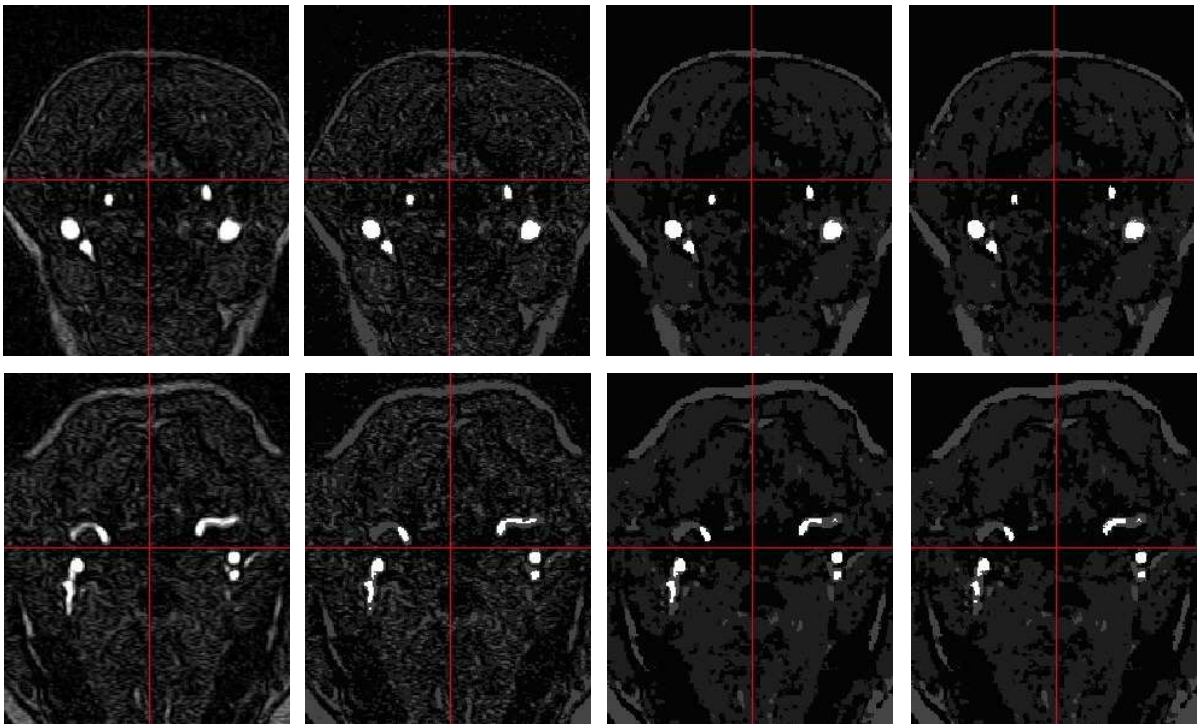

Figure 4: Segmentation for a CT angiography.

If one or more vertices have values greater than the iso-surface of interest and one or more have smaller values, then we can say that the cube is intersected by the iso-surface of interest.

By determining the points over the edges of the cube (using linear interpolation of the vertices values) where the iso-surface passes we can generate between 1 and 4 triangles (depending on how this voxel is intersected by the surface) for every cube that approximate the surface passing through it. Joining all the generated triangles we obtain a triangulation (an approximation) for the iso-surface of interest.

6.2.1. Example 1

In the case of virtual surgery, for instance neurosurgery, image segmentation and surface reconstruction is widely used. In this case the surgeon (in real surgeries) or a student (in training drills) have access to the 3D geometry via VR glasses or inside a CAVE (Computer Automatic Virtual Environment). In both cases the organs geometry must be reconstructed, and it is vital that the "virtual organs" represent the dimensions and shape of the real organs. In Figure 5 is shown the 3D reconstruction corresponding to example presented in section 6.1.2.

6.2.2. Example 2

Another application of this techniques is in the area of hemodynamics. In example was presented the segmentation of a real carotid based on a CT angiography. This three-dimensional model will be used to solve fully developed fluid dynamics equations. As shown in Figure 6 (semi-transparent white), the artery wall was reconstructed allowing us to enrich our models with the information of the wall thickness. As the geometries where obtained directly from patient data, this models can be used to study complex patient specific hemodynamic characteristics. By means of this simulation results, physicians can diagnose a cardiovascular disease in a non invasive way. In figure 6 is shown the 3D reconstruction corresponding

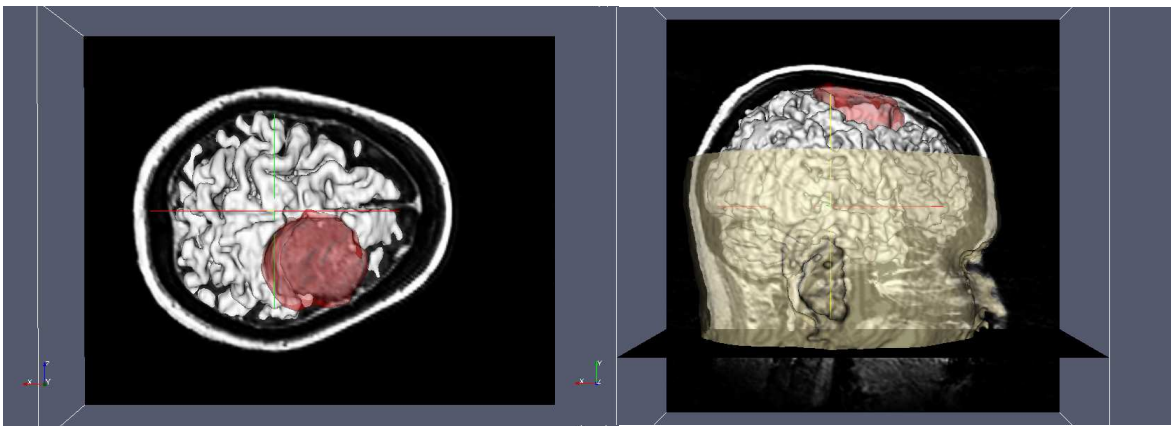

Figure 5: Tree-dimensional reconstruction of the head with a brain tumor.

to the example presented in section 6.1.3.

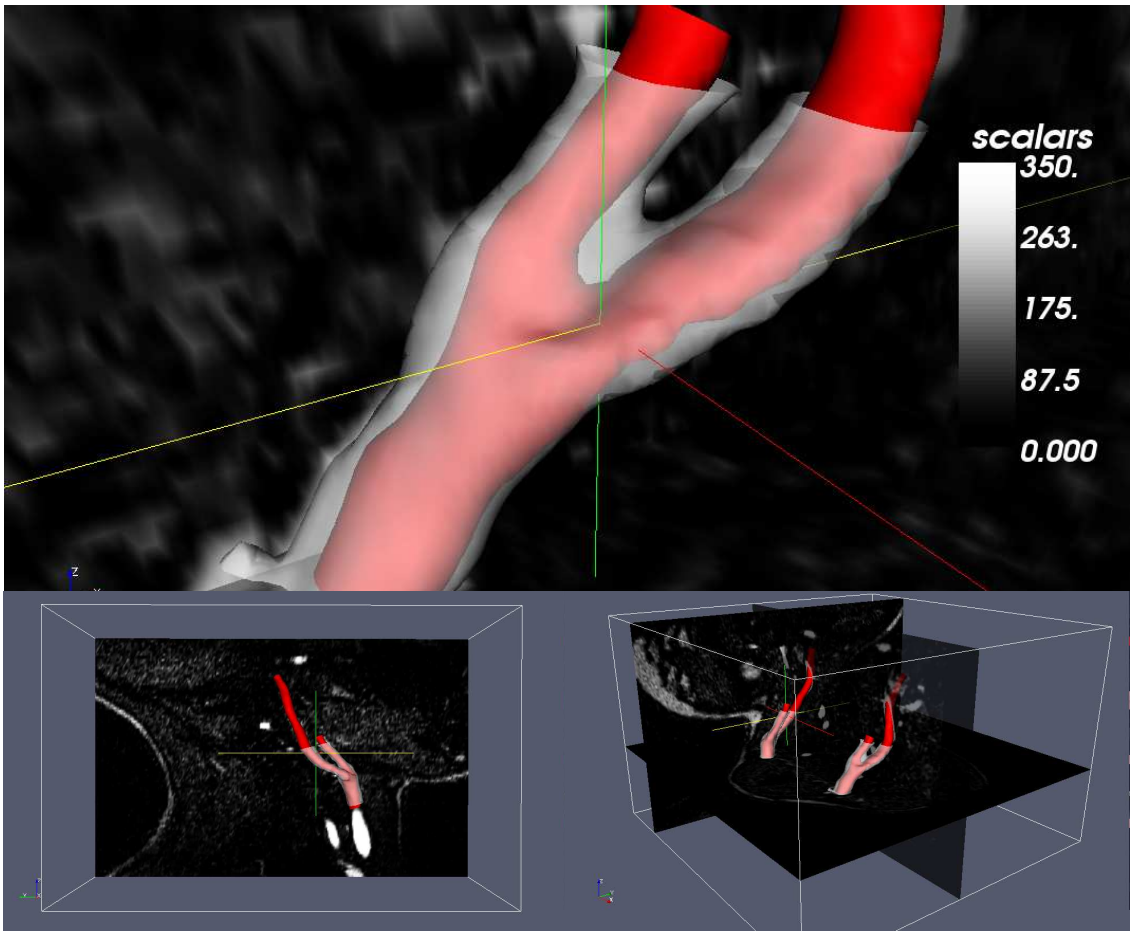

Figure 6: Tree-dimensional reconstruction of a real the carotid artery.

7. Conclusions

We presented in this work a segmentation algorithm based on the well known concept of topological derivative. We computed the topological derivative for an appropriate functional associated to the image indicating the *cost* endowed to a specific image segmentation.

In the Continuum Sensitivity Analysis problem it was necessary to solve a differential equation for an unknown field u defined over Ω before the evaluation of the topological derivative. On the other hand, in this new problem a discrete representation of the solution is given and the problem reduces to calculate the topological derivative given by the difference between two cost function instances.

Different alternatives for the algorithm were tested. The outcomes of these experiments were significantly different from one another. When the parameter $\theta \approx 1$, we recuperate the result of a threshold filter. Nevertheless, when $\theta \approx 0$ ($\theta \ll 1$) we get better results eliminating noise and unwonted features. Using this algorithm was possible to reconstruct two carotids and the artery walls from an angiography. This algorithm was also used to reconstruct a normal brain from an head MRI. Also was reconstructed, from another MRI, a diseased brain with a tumor as well as the tumor itself. This algorithm is straight-forward to be implemented and produces good quality segmentations with very little additional information and almost no user interaction. Finally, this approach needs no additional information (like seed points), besides the set of classes $\mathcal{C}$, to start the segmentation algorithm.

8. Software
This tests were implemented and run using the software Skully-Doo. Source code, Windows binaries and data files are available on the web site (http://www.skullydoo.com.ar or http://skullydoo.sourceforge.net).

9. Acknowledgments
This research was partly supported by the brazilian agencies CNPq/FAPERJ-PRONEX, under Grant E-26/171.199/2003. Ignacio Larrabide was partly supported the brazilian agency CNPq (141336/2003-0). The support from these agencies is greatly appreciated.

References

[1] Boscolo R., Brown M. S., McNitt-Gray M. F., Medical Image Segmentation with Knowledge-guided Robust Active Contours - Radiographics 22(2):437-448. 2002.

[2] Céa J. , Garreau S. , Ph. Guillaume & M. Masmoudi. The Shape and Topological Optimizations Connection. *Computer Methods in Applied Mechanics and Engineering*, 188:713-726, 2000.

[3] Neittaanmäki P. *et alli* (eds.). *ECCOMAS 2004, Mini-symposium on Topological Sensitivity Analysis: Theory and Applications*, Jyväskylä, Finland, 2004.

[4] Eschenauer H.A., Kobelev V.V. & Schumacher A. Bubble Method for Topology and Shape Optimization of Structures. *Structural Optimization*, 8:42-51, 1994.

[5] Gonzalez C.R., Woods R.E., Digital Image Processing - Second Edition, Prentice Hall, 2001.

[6] Held K., Kops E.R., Krause B.J., Wells W.M. 3rd, Kikinis R., Muller-Gartner H.W. Markov random field segmentation of brain MR images. IEEE Trans Med Imaging, 16(6):878-886, 1997.

[7] Hohne K.H., Fuchs H., Pizer S.M. 3D imaging in medicine: algorithms, systems, applications. New York, NY: Springer-Verlag, 1990.

[8] Jain A.K., Fundamentals of Digital Image Processing, Prentice Hall, 1989, ISBN 0-13-336165-9

[9] Li H., Deklerck R., De Cuyper B., Hermanus A., Nyssen E., Cornelis J.. Object recognition in brain CT-scans: knowledge-based fusion of data from multiple feature extractors. IEEE Trans Med Imaging, 14:212-229, 1995.

[10] Novotny A.A. , Feijóo R.A., Padra C. & Taroco E. Topological Sensitivity Analysis. *Computer Methods in Applied Mechanics and Engineering*, 192:803-829, 2003.

[11] Sethian J.A., Level Set Methods and Fast Marching Methods. Published by Cambridge University Press, 1999.

[12] Malladi R., and Sethian J.A. Level Set Methods for Curvature Flow, Image Enhancement, and Shape Recovery in Medical Images. Proc. of Conf. on Visualization and Mathematics, June 1995, Berlin, Germany, Springer-Verlag, Heidelberg, Germany, 329-345, 1997.

[13] Sokolowski J. & Żochowski A. On the Topological Derivative in Shape Optimization. *SIAM Journal on Control and Optimization*, 37:1251-1272, 1999.

[14] Suri J., Singh S., Setarehdan K., eds. Advanced algorithmic approaches to medical image segmentation: state-of-the-art applications in cardiology, neurology, mammography and pathology. New York, NY: Springer-Verlag, 2001.

[15] Xu C., Pham D.L., Rettmann M.E., Yu D.N., Prince J.L. Reconstruction of the Human Cerebral Cortex from Magnetic Resonance Images. IEEE Transactions on Medical Imaging, 18(6):467-480, 1999.

[16] Xu C., Pham D.L., Prince J.L. Medical Image Segmentation Using Deformable Models. SPIE Handbook on Medical Imaging - Volume III: Medical Image Analysis, edited by J.M. Fitzpatrick and M. Sonka, 2000.

[17] Zhang Y., Brady M., Smith S. Segmentation of Brain MR Images Through a Hidden Markov Random Field Model and the Expectation-Maximization Algorithm. IEEE Transactions on Medical Imaging, 20(1):45-57, 2001.